RSC Advances

PAPER

View Article Online
View Journal | View Issue

Cite this: *RSC Adv.*, 2016, **6**, 4237

DNA and BSA binding, anticancer and antimicrobial properties of Co(II), Co(II/III), Cu(II) and Ag(I) complexes of arylhydrazones of barbituric acid†

Jessica Palmucci,[ab] Kamran T. Mahmudov,*[ac] M. Fátima C. Guedes da Silva,*[a] Fabio Marchetti,[b] Claudio Pettinari,[d] Dezemona Petrelli,[e] Luca A. Vitali,[f] Luana Quassinti,[f] Massimo Bramucci,[f] Giulio Lupidi*[f] and Armando J. L. Pombeiro*[a]

Received 29th September 2015
Accepted 15th December 2015

DOI: 10.1039/c5ra20157h

www.rsc.org/advances

Two new cocrystalline compounds, (Hen)(H_2L^2)·2/3H_2O (**2**) and (Him)(H_3L^3)·2H_2O (**8**), were prepared by the reaction of 5-(2-(4-chlorophenyl)hydrazono)pyrimidine-2,4,6(1*H*,3*H*,5*H*)-trione (H_3L^2) and the sodium salt of 2-(2-(2,4,6-trioxotetrahydropyrimidin-5(2*H*)-ylidene)hydrazinyl)benzenesulfonic acid (H_4L^3), [Na(H_3L^3)(μ-H_2O)(H_2O)$_2$]$_2$ (**1**) with protonated ethylenediamine (Hen) and imidazole (Him), respectively. By using 5-(2-(2-hydroxyphenyl)hydrazono)pyrimidine-2,4,6(1*H*,3*H*,5*H*)-trione (H_4L^1) and **1**, several known Cu^{II}, Co^{II}, $Co^{II/III}$ and new Ag^{I} complexes, [Cu(H_2L^1)(H_2O)(im)]·3H_2O (**3**), [Co(H_2O)$_6$]-[Co(H_2L^1)$_2$]$_2$·8H_2O (**4**), [Co(H_2L^3)(im)$_3$] (**5**), [Cu(H_2L^3)(im)$_2$]·H_2O (**6**), [Ag(H_2O)(μ-H_3L^3)]$_n$ (**7**) and [Co(H_2O)$_6$]-[H_3L^3]$_2$·8H_2O (**9**), were also prepared in order to study their DNA and BSA binding, anticancer and antimicrobial properties. The complexes are able to interact with DNA and BSA with high binding constant values. In particular, complex **4** strongly intercalates DNA and binds BSA. The antimicrobial activity of all compounds, determined against a panel of reference bacterial and fungal strains, indicates that only **2** and **7** possess antimicrobial activity. The same compounds **2** and **7** show a pronounced antiproliferative activity against the human tumor cell lines A375, MDA-MB 231 and HCT116.

Introduction

Although barbituric acid is pharmacologically inactive, its derivatives possess very interesting pharmaceutical properties and can lead to drugs that act as central nervous system depressants, as sedatives (in small doses)/hypnotic (in larger doses) pharmaceuticals, anticonvulsants and anesthetics.[1–5] Currently, therapeutic applications of barbiturates are expanding in connection with their antitumor, anti-invasive and anti-angiogenic effects.[2–5] The pharmaceutical properties of barbiturates mainly depend on the side groups attached to the C5 atom of the pyrimidine ring (Scheme 1a).[1–5] Several methods for the modification/functionalization of barbituric acid have been reported,[6–11] and one of the most common and widely used concerns the Japp–Klingemann reaction, in which barbituric acid reacts with diazonium salts leading to arylhydrazones of barbituric acid (AHBAs) (Scheme 1b) in a basic medium.[6,8] However, to our knowledge, pharmaceutical properties of AHBAs have not yet been studied, what is explored in this work, including their cocrystals and metal complexes.

Poor aqueous solubility is one of the most serious formulation challenges facing the pharmaceutical industry today.

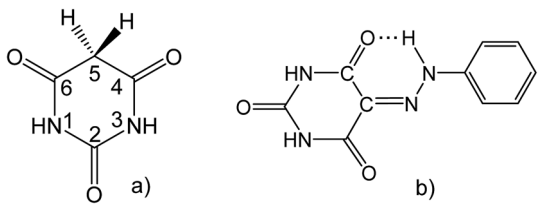

Scheme 1 Molecular structure of barbituric acid (a) and AHBAs (b).

[a]*Centro de Química Estrutural, Instituto Superior Técnico, Universidade de Lisboa, Av. Rovisco Pais, 1049-001 Lisbon, Portugal. E-mail: kamran_chem@mail.ru; kamran_chem@yahoo.com; fatima.guedes@tecnico.ulisboa.pt; pombeiro@tecnico.ulisboa.pt*

[b]*School of Science and Technology, University of Camerino, Chemistry Section, via S. Agostino 1, 62032 Camerino, Italy*

[c]*Department of Chemistry, Baku State University, Z. Xalilov Str. 23, Az 1148 Baku, Azerbaijan*

[d]*School of Pharmacy, University of Camerino, Chemistry Section, via S. Agostino 1, 62032 Camerino, Italy*

[e]*School of Biosciences and Veterinary Medicine, University of Camerino, Piazza dei Costanti 4, 62032 Camerino, Italy*

[f]*School of Pharmacy, University of Camerino, Biological Section, via Gentile III da Varano, 62032 Camerino, Italy. E-mail: giulio.lupidi@unicam.it*

† Electronic supplementary information (ESI) available: Crystal data, experimental parameters and selected details of the refinement calculations (for **2** and **8**), electronic absorption and emission fluorescence spectra of compounds **1–9**. CCDC 1055318, 1055323 and 1055324 contain the supplementary crystallographic data for compounds **2**, **7** and **8**, respectively. For ESI and crystallographic data in CIF or other electronic format see DOI: 10.1039/c5ra20157h

Approximately 40% of the drugs discovered through combinatorial chemistry and high throughput screening have an aqueous solubility of less than 10 μM.[12–14] Limited aqueous solubility of drug molecules can lead to poor bioavailability and constitutes a significant risk factor in low oral absorption.[15] A number of strategies have been employed for increasing the dissolution rate of poorly aqueous soluble pharmaceuticals, specifically in solid dosage formulations, the most applied technique for dissolution enhancement being cocrystal/salt formation.[16,17] As far as we know, before the current work, cocrystals of AHBAs had not yet been isolated and structurally characterized, and their antimicrobial and antitumor activity and DNA/protein binding studies had not been performed.

Thus, in this work we focused on the following aims: (i) synthesis of new AHBA ligands and their cocrystals with ethylenediamine (en) and imidazole (im); (ii) preparation of new Ag^{I} and known water soluble Co^{II}, $Co^{II/III}$ and Cu^{II}–AHBA complexes (Scheme 2);[18] (iii) evaluation of the antimicrobial and

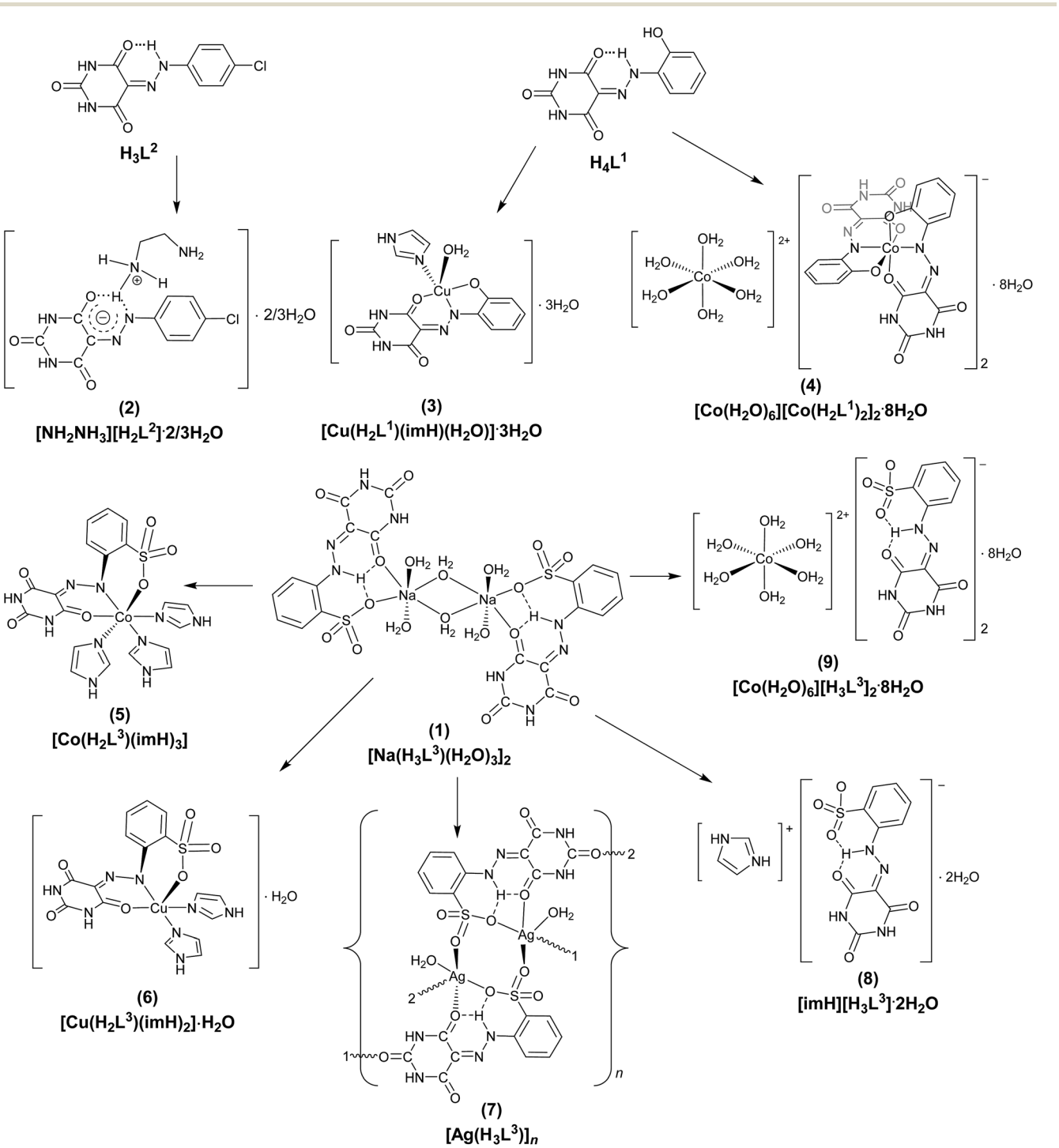

Scheme 2 Schematic representations of H_4L^1, H_3L^2 and **1**–**9**.

antiproliferative activities all AHBA ligands and their cocrystals and Co^{II}, $Co^{II/III}$, Cu^{II} and Ag^{I} complexes; (iv) investigation of the binding mode of AHBAs and their cocrystals and complexes to DNA and BSA albumin, that should play a role in the pharmacokinetics and pharmacodynamics of such potential drugs.

Results and discussion

Synthesis and characterization of AHBA ligands their cocrystals and $Co^{II/III}$, Cu^{II} and Ag^{I} complexes

Water soluble 5-(2-(2-hydroxyphenyl)hydrazono)pyrimidine-2,4,6(1*H*,3*H*,5*H*)-trione ($\mathbf{H_4L^1}$), sodium salt of 2-(2-(2,4,6-trioxotetrahydropyrimidin-5(2*H*)-ylidene)hydrazinyl)benzene-sulfonic acid ($\mathbf{H_4L^3}$), $[Na(H_3L^3)(\mu\text{-}H_2O)(H_2O)_2]_2$ (**1**), $[Cu(H_2L^1)(H_2O)(im)]\cdot 3H_2O$ (**3**), $[Co(H_2O)_6][Co(H_2L^1)_2]_2\cdot 8H_2O$ (**4**), $[Co(H_2L^3)(im)_3]$ (**5**), $[Cu(H_2L^3)(im)_2]\cdot H_2O$ (**6**) and $[Co(H_2O)_6][H_3L^3]_2\cdot 8H_2O$ (**9**) (Scheme 2) were reported earlier by us,[18] and hence will not be discussed.

5-(2-(4-Chlorophenyl)hydrazono)pyrimidine-2,4,6(1*H*,3*H*,5*H*)-trione ($\mathbf{H_3L^2}$) (Scheme 2) was prepared by a modified known[18–22] aqueous diazotization of 4-chloroaniline and subsequent coupling with barbituric acid in basic medium. $\mathbf{H_3L^2}$ is highly soluble in DMSO, DMF, water, methanol, acetone and acetonitrile. The ^{1}H and ^{13}C-NMR spectra of $\mathbf{H_3L^2}$ support the hydrazone form and =N–NH– signal is observed at δ 14.03 in the ^{1}H-NMR spectrum, while the ^{13}C-NMR spectrum shows two separate singlets for the C=O and C=O···H of pyrimidine moiety at δ 159.76 and 161.92, respectively (Fig. 1S and 2S†). The IR spectrum of $\mathbf{H_3L^2}$ shows ν(NH) vibrations at 3260, 3085 and 2813 cm^{-1}, while ν(C=O) at 1753 and 1653, ν(C=O···H) at 1588 and ν(C=N) at 1513 cm^{-1} (Fig. 3S†), supporting the existence of the H-bonded hydrazone structure in the solid state.

Cocrystals of $(Hen)(H_2L^2)\cdot 2/3H_2O$ (**2**) were obtained from reaction of $\mathbf{H_3L^2}$ with ethylenediamine (en) in methanol (Schemes 2 and 1S†). The IR spectrum of **2** displays ν(C=O) at 1693 cm^{-1}, value that is significantly shifted in relation to that (1753 cm^{-1}) of the free ligand (Fig. 4S†). The ^{1}H-NMR spectrum of **2** in DMSO-d^6 solution at room temperature confirms the disappearance of the hydrazone proton (Fig. 5S and 6S†). The ESI mass spectrum of **2** dissolved in methanol shows the parent peak at $m/z = 327.2$ $[C_{12}H_{15}ClN_6O_3 + H]^+$. Elemental analyses are consistent with the proposed formulation, which is also supported by X-ray crystallography (see below).

Another cocrystalinde compound, $[(Him)(H_3L^3)]\cdot 2H_2O$ (**8**), was isolated by treatment of **1** with imidazole (im) in the presence of HNO_3 in methanol (Scheme 2). Whereas, the first Ag^{I} complex with an AHBA ligand, $[Ag(H_2O)(\mu\text{-}H_3L^3)]_n$ (**7**), is obtained in acidic medium (with addition of HNO_3) from reaction of **1** with $AgNO_3$ in acetone–water mixture (4 : 1, v/v) at room temperature (Scheme 2). Both compounds, **7** and **8**, were characterized by elemental analysis, ^{1}H and ^{13}C NMR spectroscopies (Fig. 7S–12S†), ESI-MS, IR spectroscopy and single crystal X-ray diffraction. In the IR spectra of **7** and **8**, the ν(C=O) signal appears at 1689 and 1698 cm^{-1} (Fig. 13S and 14S†), respectively, values that are significantly shifted in relation to the corresponding signal of **1** (1677 cm^{-1}, Fig. 15S†). The ESI mass spectra of **7** and **8** dissolved in CH_3OH show the peaks at m/z = 839.1 $[2\{[Ag(H_2O)(\mu\text{-}H_3L^3)]_n\} - 2H_2O + H]^+$ and 312.1 $[H_3L^3 + H]^+$. In the ^{1}H NMR spectra of **7** and **8**, the hydrazone protons are observed at 14.78 and 14.79 ppm, respectively (Fig. 7S and 9S†). Elemental analyses are consistent with the proposed formulations which are also proved by X-ray analysis (see below). Both compounds are soluble in polar solvents such as water, methanol, DMF and DMSO.

X-ray diffraction analyses

Crystals of **2** and **8** suitable for X-ray diffraction analysis were obtained upon crystallization from methanol or water–acetone mixtures (1 : 4, v/v) (**7**). Representative plots of **2**, **7** and **8** are depicted in Fig. 1. Crystallographic data and refinement parameters are given in Table 1S,† selected bond distances and angles in Table 2S.† H-contacts for **2**, **7** and **8** are outlined in Table 3S† and depicted in Fig. 16S–19S†.

In **2** and **8** the $(H_2L^2)^-$ or $(H_3L^3)^-$ species cocrystallized with monoprotonated ethylene diamine (**2**) or imidazolium (**8**) cations, respectively, apart from two water molecules, and can be roughly planar (in **8**) or present a considerable twisting (in **2**) as measured by the angles between the least square plane of the heteronuclear ring (plane *H*) and the least square plane of the phenyl ring (plane *P*; Table 3S†).

Compound **2** crystallizes in the monoclinic space group *P*21/*c* with three monoprotonated ethylene diamines, three $(H_2L^2)^-$ anions and two water molecules. Due to deprotonation of hydrazone unit of $\mathbf{H_3L^2}$ by en, its "resonance assisted hydrogen bond" (RAHB)[7] system is converted into "charge assisted hydrogen bond" (CAHB)[7] (Scheme 1S†), with medium-to-weak intermolecular hydrogen-bond contacts involving the $(H_2L^2)^-$ monoanion varying in the (donor···acceptor) range distances of 2.785(8)–3.296(8) Å (Table 3S†). Together with keto-O atoms, every hydrazo/azo group of $(H_2L^2)^-$ in **2** acts as acceptor from two Hen^+ or from one of these cations and a molecule of water, to form two (or even three) bifurcated hydrogen bonds (Fig. 16S and Table 3S†). The nitrogen and oxygen atoms of pyrimidine trione moieties of $(H_2L^2)^-$ are further linked *via* intermolecular H-contacts giving rise to an intricate 3D network (Fig. 17S†).

The asymmetric unit of **7** contains one Ag^{I} cation, a $(H_3L^3)^-$ anion and a coordinated water molecule. The structure is a 1D polymer that runs along the crystallographic *b* direction with the metal cation adopting a distorted square pyramidal geometry ($\tau_5 = 0.35$)[23] filled by the oxygen atom from water, two $O_{sulfonyl}$-atoms and two O_{ketone}-atoms from three adjacent symmetry generated hydrazone moieties (Fig. 18S†). An interesting feature of polymer **7** arises from the μ-OOSO bridging mode of the sulfonyl groups of the organic ligands which results in the generation of $\{Ag_2S_2O_4\}$ dimetallic cores (Fig. 19S†). These cores are then doubly bound by two O_{ketone}-atoms from the pyrimidine trione moieties thus giving rise to an infinite 1D double chain. Therefore, this double chain comprises additional cavities formed by repeating 12-membered dimetallic $-\{AgO_{ketone}CNCO_{ketone}\}_2-$, and 10-membered monometallic $-\{AgO_{sulfonyl}SC_2N_2C_2O_{ketone}\}-$ rings. In **7** the $(H_3L^3)^-$ anion preserves the strong RAHB linking the NH-moiety of the hydrazone unit (N1–H1N) in a three-centered interaction with

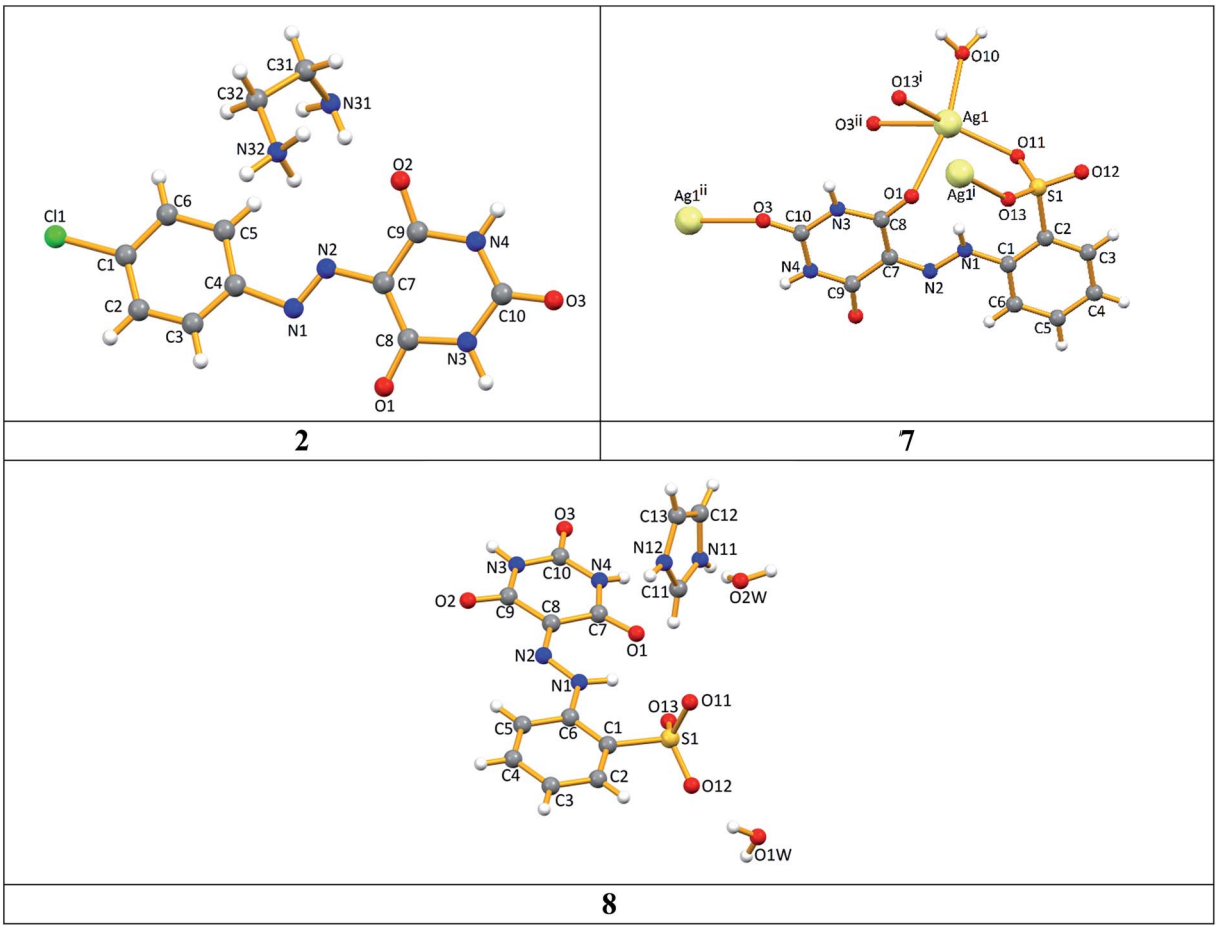

Fig. 1 X-ray molecular structures of **2**, **7** and **8** with atom numbering schemes. In **2**, only one hydrazine anion and one ethylenediammonium cation is shown.

coordinated O_{ketone}- and $O_{sulfonyl}$-atoms. The non-coordinated $O_{sulfonyl}$-atom (O12) is involved in an intra-chain H-bond contact acting as acceptor towards HN(3) (donor site) of pyrimidine moiety.

The structure of **8** contains three-centred RAHB/CAHB interactions[7] in the anionic hydrazone units involving the O_{ketone}- and $O_{sulfonyl}$-atoms, which relates to the synergistic mutual reinforcement of intramolecular hydrogen bonding due to π-electron delocalization. The typical double bond lengths of $C_{pyrimidine}$–$N_{hydrazone}$ in the structure of **8** [1.326(4) Å] and the formation of intramolecular N–H···O RAHB contacts indicate that hydrazone is the preferred tautomeric form in these cases. The structure of **8** contains trapped water molecules, which interact among themselves and with the imidazolium and pyrimidine trione moiety *via* intermolecular hydrogen bonds. Such interactions, together with others involving the O- and N-atoms of pyrimidine trione rings (Table 3S and Fig. 20S†), give rise to intricate 3D supramolecular frameworks.

Electronic absorption spectra. The electronic absorption spectra of the complexes **1–9** and the free proligands $\mathbf{H_4L^1}$ and $\mathbf{H_3L^2}$ have been recorded in DMSO (**2–9**, $\mathbf{H_4L^1}$ and $\mathbf{H_3L^2}$) and water solution (**1**) and all the spectra are reported in Fig. 21S (ESI†). The wavelength (λ_{max}) and molar absorption values (ε) of all free ligands, their metal complexes and cocrystals in the UV-vis region 220–600 nm are reported in Table 4S (ESI†). In the spectra of $\mathbf{H_4L^1}$ and $\mathbf{H_3L^2}$ the bands at 262–266 nm are due to π–π* electronic transition in C=O, while the bands at 388–414 nm are mainly of n–π* type in N=N.[24–26] Similarly the sodium complex **1** shows analogous features, even if the band at the lower wavelength seems splitted into two very close absorptions.

With respect to $\mathbf{H_4L^1}$, in the spectra of its complexes **3** and **4**, containing Cu(II) and Co(II/III) respectively, a new broad and very intense absorption band appears in the 420–480 nm range, which suggests n–π* and π–π* electronic transitions in the obtained compounds. Thus, new band can be attributed to a deprotonated form of the ligand moiety arising upon coordination to a metal centre and can be assigned to electronic transitions to bring about the conjugation between the metallocycles and the aromatic ring system.

The spectra of metal the complexes **5–9** are essentially similar to that of the ligand in the sodium salt **1**, apart for the Co(II) and Cu(II) complexes **5** and **6**, respectively, where a broadening of the band at lower wavelength is observed, due to an additional band partially obscured by the formed one. No d–d or CT transitions were observed in any of the Co^{II} and Cu^{II} complexes and this may be due to the weakness of the bands at

such low concentrations of the solutions (*ca.* 10^{-4} M) or because they are obscured by the intense bands.

DNA-binding mode and affinity. The mechanisms of DNA-binding and behaviour of metal complexes, as novel potential therapeutic agents, are strongly attributed to the size, shape, and planarity of the intercalative ligands. Metal complexes can bind to DNA *via* both covalent and/or non-covalent interactions. In covalent binding the labile ligand of the complexes is replaced by a nitrogen atom from a DNA base such as guanine N7. Non-covalent DNA interactions include intercalative, electrostatic and groove (surface) binding. Intercalation can involve the partial insertion of aromatic heterocyclic rings of the ligands between the DNA base pairs.[27] When metal complexes intercalate to the base pair of DNA, the π^* orbital of the intercalated ligands in the complexes can couple with π orbitals of the base pairs, thus decreasing the π–π^* transition energies. On the other hand, the coupling π^* orbital can be partially filled by electrons, thus decreasing the transition probabilities.[28] Thus, some basic interaction studies of metal (or ligands)-complex–DNA are of relevance and we have used different methods to evaluate the DNA binding affinity of the complexes **1–9** and the proligands $\mathbf{H_4L^1}$ and $\mathbf{H_3L^2}$ explored in this work.

Electronic absorption titration. Electronic absorption spectroscopy is universally employed to examine the binding mode of DNA with small molecules. The interaction of such molecules with DNA is often characterized through absorption spectral titration, followed by the changes in the absorbance and shift in the wavelength. The absorption spectra of complex **4** in the absence and presence of calf thymus DNA (ct-DNA), is given in Fig. 2 while the results obtained for the titration of all complexes and proligands are reported in Fig. 22S (ESI†).

As reported in Fig. 2, fixed amounts of complex **4** were titrated with increasing amount of ct-DNA (0–26 μM), resulting in an overall hyperchromism at the intraligand absorption bands in the 240–280 nm range of the complex. In general, the "hyperchromic effect" is related to corresponding changes of DNA on its conformation and structure, after coordination with metal complexes.[29] Hypochromism results from contraction of DNA in the helix axis, while hyperchromism arises from the damage of DNA double helix structure.[30,31] An "hyperchromic effect" has been observed for all the tested compounds, while a moderate red shift of 1–4 nm was observed only for complexes **5** and **7**. The hyperchromic effect with red shift seems to suggest that complexes **5** and **7** bind to DNA by external contact possibly *via* electrostatic binding, as previously observed for other metal complexes.[32]

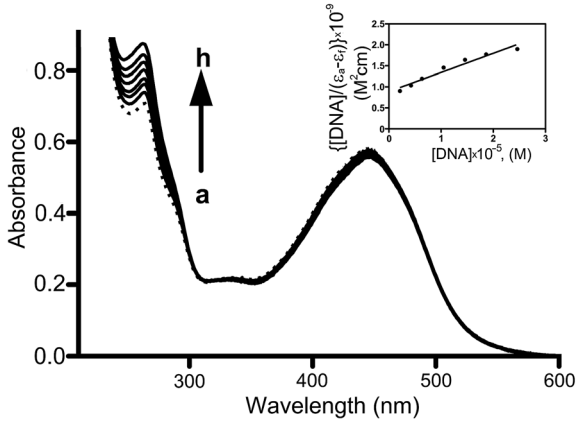

Fig. 2 Absorption spectral traces of complex **4** buffer (10 mM, pH 7.2) after gradual addition of calf thymus DNA (from a = 0 to h = 24 μM). Inset shows the plot of $[DNA]/|\varepsilon_a - \varepsilon_f|$ *vs.* [DNA] (eqn (1) in ESI†).

For complexes **1**, **3**, **4**, **6**, **8** and **9**, or proligands $\mathbf{H_4L^1}$ and $\mathbf{H_3L^2}$, no shift of the absorption maximum was observed and this behaviour can be probably related to a different DNA binding propensity. To further evaluate the binding affinity of complexes and cocrystals with ct-DNA, the intrinsic binding constant has also been determined by using eqn (1) (ESI†), detecting the changes of absorbance for of different concentrations of ct-DNA. The values of the binding constant K_b, obtained from for compounds **1–9** are reported in Table 1 and can be resumed according to the following trend: $\mathbf{4} \gg \mathbf{2} > \mathbf{7} > \mathbf{3} \approx \mathbf{H_4L^1} \approx \mathbf{8} \approx \mathbf{5} \approx \mathbf{9} > \mathbf{6} \approx \mathbf{H_3L^1} \approx \mathbf{1}$.

Competitive studies with EB. The measurement of the ability of a complex to affect the ethidium bromide (EB) fluorescence intensity in the EB–ct-DNA adducts can also be used to determine of the affinity of the complex for DNA.[33] EB is a sensitive fluorescence probe, emitting intense fluorescence at about 600 nm in the presence of DNA, due to its strong intercalation between the adjacent DNA base pairs, and the enhanced fluorescence could be quenched by the addition of another competitive binding molecule. If a molecule can replace EB from the EB–DNA complex, a decrease of fluorescence of the solution is observed due to the fact that free EB molecules are readily quenched by the surrounding water molecules. Two mechanisms have been proposed to account for the reduction in the emission intensity: the replacement of molecular fluorophores (EB in this case) and/or electron transfer.[34,35]

Fig. 3 reports the emission spectra of the EB–ct-DNA in the presence of increasing amounts of complex **4**. The addition of **4** (different concentrations) to the EB-bound ct-DNA solution caused a reduction in emission intensity, indicating that complex **4** substitutes ct-DNA-bound EB and binds to ct-DNA with different affinity. In order to understand quantitatively the magnitude of the binding strength of complexes **1–9** and proligands $\mathbf{H_4L^1}$ and $\mathbf{H_3L^2}$ with ct-DNA, the quenching ability has been then analyzed by the Stern–Volmer equation and K_{SV} values are shown in Table 1. From data on Table 1 a low correlation between K_b and K_{SV} values was observed, probably due to the different sensitivity of the two techniques used. Additionally we have evaluated the binding constant K_{app} (Table 1), and the values obtained for compounds **3**, **4**, **5**, **9** and the proligand $\mathbf{H_4L^1}$ suggest that they intercalated strongly to DNA. A similar mechanism is hypothesized for the other compounds and the free proligand that bind to DNA with lower affinity.

Fig. 23S (ESI†) reports the emission quenching spectra of EB–ct-DNA solutions in the presence of all complexes and proligands. Data from Table 1 suggest a stronger interaction of complexes **3**, **4**, **5** and **9** with EB–ct-DNA ($\mathbf{4} > \mathbf{5} \approx \mathbf{9} > \mathbf{3} > \mathbf{H_4L^1}$), than the remaining compounds, showing a lower affinity for the EB–ct-DNA complex in the following order: $\mathbf{6} \approx \mathbf{2} > \mathbf{8} > \mathbf{H_3L^2} > \mathbf{7}$.

Table 1 Values of binding constants with DNA and BSA for the interaction of complexes **1–9** and proligands H_4L^1 and H_3L^2

Compound	BSA binding $K_{SV} \times 10^4\ M^{-1}$	BSA binding $K_q \times 10^{13}\ M^{-1}\ s^{-1}$	ct-DNA binding $K_b \times 10^3\ M^{-1}$	EB–ct-DNA binding $K_{SV} \times 10^3\ M^{-1}$	EB–ct-DNA binding $K_{app} \times 10^5\ M^{-1}$	DAPI–ct-DNA binding $K_{SV} \times 10^3\ M^{-1}$
1	8.80(±0.36)	0.88(±0.03)	0.75(±0.24)	ND	ND	18.65(±0.20)
2	16.42(±0.40)	1.64(±0.04)	13.6(±0.27)	4.95(±0.24)	2.47	13.61(±0.78)
3	10.48(±0.22)	1.04(±0.02)	1.76(±0.34)	11.73(±0.12)	5.86	9.45(±0.36)
4	96.82(±0.40)	9.68(±0.04)	54.9(±0.10)	28.54(±0.05)	14.27	70.05(±2.51)
5	26.31(±0.12)	2.63(±0.02)	1.14(±0.36)	21.66(±0.10)	10.83	13.47(±0.10)
6	29.64(±0.85)	2.96(±0.08)	0.85(±0.21)	5.42(±0.30)	2.71	13.38(±0.21)
7	17.28(±0.80)	1.72(±0.08)	3.33(±0.60)	0.53(±0.02)	0.26	8.55(±1.20)
8	25.55(±0.30)	2.55(±0.03)	1.17(±0.44)	1.56(±0.25)	0.78	28.60(±0.06)
9	16.50(±0.90)	1.65(±0.09)	1.12(±0.35)	21.84(±0.07)	1.09	21.90(±0.60)
H_3L^2	18.24(±1.76)	1.82(±0.17)	0.78(±0.21)	0.88(±0.06)	0.44	1.39(±0.21)
H_4L^1	16.46(±1.16)	1.64(±0.11)	1.36(±0.40)	8.93(±0.61)	4.46	27.33(±0.52)

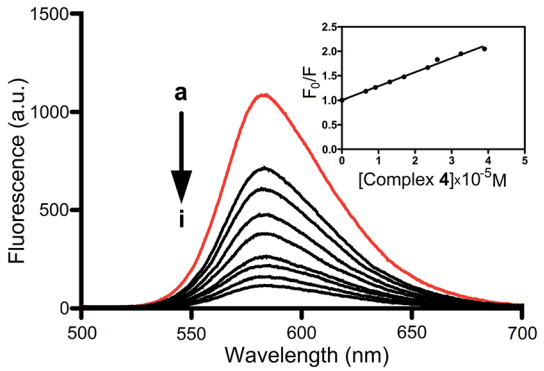

Fig. 3 Emission spectra of EB bound to ct-DNA in the presence of complex **4** with increasing concentration (from a = 0 to I = 39 μM); ([EB] = 5 μM, [ct-DNA] = 50 μM). Inset: Stern–Volmer plot of F_0/F *vs.* [complex **4**] for the titration of EB–ct-DNA system with complex **4**.

Moreover, the high K_{app} values obtained (about $10^5\ M^{-1}$) suggest that our compounds intercalate strongly to DNA with similar mechanism, *i.e.* through the replacement of EB from DNA, but with different affinity.

Competitive studies with DAPI. DAPI is a very well known fluorogenic probe that binds to the minor groove of DNA.[36] However, in the presence of another molecular species able to bind to the DNA minor groove, there would be competition between this species and DAPI, and displacement of DAPI from ct-DNA produces a decrease in the fluorescence intensity of the DAPI–ct-DNA complex.

As shown in Fig. 4, the addition of **4**, with increasing concentration, to the DAPI–ct-DNA complex reduces its fluorescence intensity, thereby clearly suggesting that complex **4** can display DAPI to a considerable extent and can be able to bind to the minor groove of DNA. Results for all complexes and proligands are reported in Fig. 24S (ESI†). Of particular interest is the behaviour of complex **7** and the cocrystalline **2**: in fact they do not decrease the fluorescence of DAPI–ct-DNA but produce an hyperchromic effect with an increase of fluorescence and a blue shift of the emission maximum. Compounds **2** and **7** interact with the system DAPI–ct-DNA with different affinity, but the presence of isosbestic points indicates an equilibrium state between the complexes and DAPI–ct-DNA (Fig. 24S†). The significant hyperchromic effects, as well as the moderate blue shift of the emission maximum, support the existence of a strong interaction between compounds **2** and **7** and the whole system DAPI–ct-DNA, without expulsion of DAPI molecules from the minor grove of DNA. A possible interaction between the metal compounds and the DAPI–ct-DNA system can be through external electrostatic interaction between the metal compounds and the DAPI–ct-DNA system. A similar situation has been recently found in the case of water-soluble tris(pyrazolyl) methanesulfonate silver(I) derivatives of *N*-methyl-1,3,5-triaza-7-hosphaadamantane salt.[37]

The Stern–Volmer quenching constants for the interaction of complexes and proligands with DAPI–ct-DNA were evaluated and reported in Table 1. The values of K_{SV} show also in this case that complex **4** has the highest affinity towards DNA. The affinity of the tested compounds follow the order **4** ≫ **8** ≈ H_4L^1

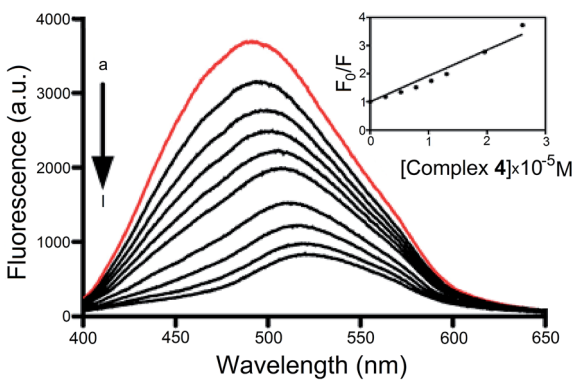

Fig. 4 Emission fluorescence spectra of DAPI–ct-DNA complex upon excitation at 338 nm in the presence of **4** with increasing concentration (from a = 0 to I = 36 μM). Experiments were performed in 10 mM phosphate buffer, pH 7.2. Inset: Stern–Volmer plot of F_0/F *vs.* [complex **4**] for the titration of DAPI–ct-DNA complex with complex **4**.

> **9** > **1** while a lower activity was observed for the remaining species (**2** ≈ **5** ≈ **6** > 3 ≈ **7** ≈ **9** > $\mathbf{H_3L^2}$). It's worth to note that, after **4**, the co-crystal **8** seems very able to display efficiently DAPI from the minor grove of DNA helix, in accordance with previous findings on several imidazolium salts.[38]

From all data of Table 1 we can conclude that complexes **3**, **4**, **5**, **6**, **7** and **8** display a very high affinity for DNA, but probably with different types of association, based on the value of their association constants. Interestingly, the Co(II) complex **4** was that with the highest activity which preferentially seems to bind to minor groove of DNA.

The highest affinity of the ionic complex **4** for both EB–ct-DNA and DAPI–ct-DNA, with respect to all other compounds, is likely related to its bulkiness, being composed by a cationic $[Co(OH_2)_6]^{2+}$ unit and two anionic $[Co(H_2L^1)_2]^-$ counterparts. Such very big system displays the highest ability, among the others, to replace EB from the major grove of DNA and also DAPI from the minor grove of DNA. Moreover, also the binding constant K_b of **4** is the highest among the others, and *ca.* 50 times higher than that exhibited by compound **9**, containing the same cationic unit $[Co(OH_2)_6]^{2+}$, but only an anionic $(H_3L^3)^-$ ligand. This means that there is a contribution of the anionic $[Co(H_2L^1)_2]^-$ unit of compound **4** in its ability to bind DNA and to replace EB and DAPI from major and minor groves, respectively. Such contribution can be tentatively explained if we consider the possibility of ionic pairs formation such as $\{[Co(OH_2)_6][Co(H_2L^1)_2]\}^+$ for compound **4** and $\{[Co(OH_2)_6](H_3L^3)\}^+$ for compound **9**, which may behave as single positive systems able to interact with the negative backbone of phosphate groups in DNA through electrostatic interactions and then intercalation. Differently to the simple anion $(H_3L^3)^-$ in compound **9**, the anionic unit $[Co(H_2L^1)_2]^-$ in compound **4** contains a d^6 low spin Co(III) center, which is able to strongly attract and concentrate the whole negative change on it, by depleting the electronic cloud from the periphery of the complex. Additionally, DNA double helix possesses many hydrogen-bonding sites positioned on the edges of the DNA bases, so that it's quite possible that the $(H_2L^1)^-$ functionalities could participate in H-bonding with the DNA base pairs and intercalate the DNA helix,[39] even if the $(H_2L^1)^-$ ligands are part of an anionic complex.

Protein binding studies. The interactions between the most abundant blood proteins, as serum albumins, and metal complexes have attracted immense interest because of their possible role in plasma delivery.[40] Their binding with a drug may actually result in an increase or decrease of the drug's efficacy, making it important to investigate the interactions of prospective drugs with serum albumins. Simple and effective methods for investigating the strength and mode of binding of small molecules to serum albumin are available.[41] BSA (bovine serum albumin) has a well-known structure consisting of a single polypeptide chain containing two tryptophan residues, that are responsible for the majority of the intrinsic fluorescence of the protein and shows a strong fluorescence emission with a peak near 340 nm upon excitation at 285 nm.[42] This emission is sensitive to the changes in the local environment of the tryptophan,[43] and can be attenuated by the binding of a small molecule at or near this residue.[44] The binding of complex **4** to BSA is reported in Fig. 5: the addition of increasing amounts of **4** decreases dramatically the intrinsic fluorescence of the protein. A similar behaviour is observed for the other complexes and proligands with BSA (Fig. 25S in ESI†). The addition of the complexes to BSA results in a large reduction in the fluorescence intensity without any shift of the emission maximum.

The Stern–Volmer constants of binding to BSA for all complexes and proligands are reported in Table 1. Complex **4** is also in this case the most active complex towards the binding to BSA, with a Stern–Volmer constant about 3 times higher than those of the other complexes.

Also in this case there is a different ability in binding BSA by the ionic compounds **4** and **9** containing the same cationic unit $[Co(OH_2)_6]^{2+}$ but two different anionic counterparts, $[Co(H_2L^1)_2]^-$ and $[(H_2L^3)]^-$. So that, even if we can imagine that the primary interaction with BSA protein chain could be with the cationic unit $[Co(OH_2)_6]^{2+}$, possibly through replacement of some water molecule from a labile d^7 Co(II) centre, we cannot exclude some steric contribution from the anionic $[Co(H_2L^1)_2]^-$ unit. Beside this, compounds **5**, **6** and **8** show essentially the same activity towards the BSA (Table 1), likely due to the hydrophobicity of substituents in the ligand and not to the type of metal in the complex. Whereas, compounds **2**, **7** and **9** bind to BSA with moderate affinity, similar to that of proligands $\mathbf{H_4L^1}$ and $\mathbf{H_3L^2}$.

It is well known that there are two quenching mechanisms involved in quenching process, which are usually classified as dynamic quenching and static quenching. Dynamic quenching refers to a process where the fluorophore and the quencher come into contact during the lifetime of the excited state, whereas static quenching refers to fluorophore–quencher complex formation.[45] According to the literature, for dynamic quenching the maximum scatter collision quenching constant of various quenchers with the biopolymer is 2.0×10^{10} M^{-1} s^{-1} [46] and the fluorescence lifetime of the biopolymer is 10^{-8} s.[47]

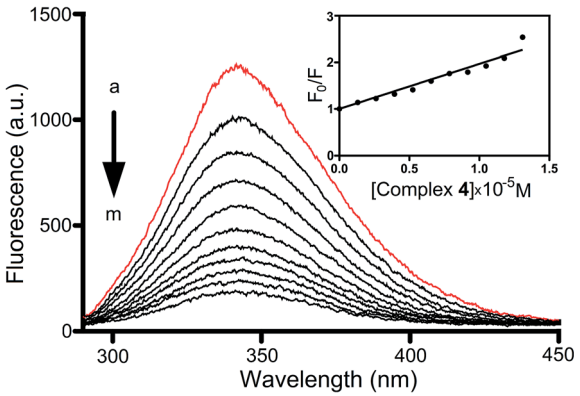

Fig. 5 Emission spectra of BSA (15×10^{-6} M) in 20 mM phosphate buffer (pH = 7.4) and 25 °C. Excitation carried out at 285 nm. The arrow (with its direction) shows that the increasing concentration of complex **4** (from a = 0 to m = 30 μM) is accompanied by a quenching of BSA fluorescence intensity. Inset, Stern–Volmer plots of F_0/F *vs.* [complex **4**] for the titration of BSA with complex **4**.

Table 2 *In vitro* cytotoxic activity of proligands H_4L^1, H_3L^2, cocrystals **2**, **8** and complexes **1**, **3–7**, **9**[a]

	Cell line (IC_{50} μM)		
	A375[b]	MDA-MB 231[c]	HCT116[d]
$\mathbf{H_4L^1}$	79.3	>100	>100
95% C.I.	68.6–82.4		
$\mathbf{H_3L^2}$	>100	>100	>100
95% C.I.			
1	>100	>100	>100
95% C.I.			
2	17.43	24.81	17.28
95% C.I.	16.60–18.31	23.10–26.66	16.74–17.83
3	>100	>100	>100
95% C.I.			
4	>100	>100	>100
95% C.I.			
5	>100	>100	>100
95% C.I.			
6	>100	>100	>100
95% C.I.			
7	0.97[e,g]	1.78[e,f]	1.14[e,f]
95% C.I.	0.93–1.00	1.65–1.91	1.04–1.17
8	>100	>100	>100
95% C.I.			
9	>100	>100	>100
95% C.I.			
$AgNO_3$	2.73	11.20	6.01
95% C.I.	2.37–2.92	9.90–12.67	5.66–6.38
Cisplatin	0.59	7.12	4.92
95% C.I.	0.51–0.71	5.99–7.62	4.51–5.50

[a] The IC_{50} value is the concentration of compound that affords a 50% reduction in cell growth (after 72 h of incubation). C.I. = confidence interval. [b] Human malignant melanoma cell line. [c] Human breast adenocarcinoma cell line. [d] Human colon carcinoma cell line. [e] The two-tailed *P* value is <0.0001, considered extremely significant (compound **7** *vs.* $AgNO_3$). [f] The two-tailed *P* value is <0.0001, considered extremely significant (compound **7** *vs.* cisplatin). [g] The two-tailed *P* value is 0.0002, considered extremely significant (compound **7** *vs.* cisplatin).

Table 1 shows the values of K_{SV} and $K_q = K_{SV}/\tau_0$. The obtained values of K_q were larger than the limiting diffusion rate constant of the biomolecule (2.0×10^{10} M^{-1} s^{-1}), which indicates that the fluorescence quenching is caused by a specific interaction between BSA and the different compounds tested. Therefore, the quenching mechanism mainly arises from the formation of BSA-complex rather than dynamic quenching. In conclusion, the static quenching is dominant in these system.[48]

Biological activity of proligands H_4L^1, H_3L^2, cocrystals 2, 8 and metal complexes 1, 3–7, 9

Antiproliferative activity. The cytotoxic activity of compounds **1–9**, silver nitrate, and cisplatin was evaluated on a selection of human tumor cell lines. A375 human malignant melanoma, MDA-MB 231 human breast adenocarcinoma, and HCT116 human colon carcinoma cell lines were tested by the MTT assay. All cell lines were submitted to increasing concentrations of compounds, in the 0.39–100 μM range, for 72 h. The IC_{50} values are shown in Table 2 and compared with $AgNO_3$. Compound **7** presents pronounced antiproliferative effects with IC_{50} values of 0.97, 1.14 and 1.78 μM, for the A375, HCT116, and MDA-MB 231 cell lines, respectively. IC_{50} values of the silver complex **7** resulted statistically significant in comparison with IC_{50} values of $AgNO_3$ and cisplatin. The cocrystalline **2** also shows antiproliferative activity on the tested cell lines, with IC_{50} values ranging from 17.3 μM to 24.8 μM for HCT116 and MDA-MB 231 cell lines, respectively. All the other compounds are inactive. $\mathbf{H_4L^1}$ shows low activity on A375 cell line.

Antimicrobial activity. The antimicrobial activity of proligands $\mathbf{H_4L^1}$ and $\mathbf{H_3L^2}$ and complexes **1–9** was determined by both disk diffusion and microdilution method. Four reference bacterial species (*S. aureus*, *E. faecalis*, *E. coli* and *P. aeruginosa*) and a fungal one (*C. albicans*) were included in this study. As shown in Tables 3 and 4, the two complexes **2** and **7** showed good antimicrobial activity against all the tested bacterial and fungal species.

One of them (**2**) is the cocrystal of $\mathbf{H_3L^2}$ with ethylenediamine (en), the second one (**7**) is the complex of **1** with silver. MIC values range from 32 to 128 for the complex **2** and from 4 to 64 μM in the case of complex **7**. Both active complexes possess a bactericidal activity. Proligands $\mathbf{H_4L^1}$ and $\mathbf{H_3L^2}$ and complexes **2–6**, **8** and **9** do not possess antimicrobial activity against the tested strains.

Table 3 Disc diffusion test of proligands H_4L^1, H_3L^2, cocrystals **2**, **8** and complexes **1**, **3–7**, **9** against a panel of reference bacterial and fungal strains. Diameters of zone inhibition are expressed in millimeters

Compound	*S. aureus* ATCC 29213	*E. faecalis* ATCC 29212	*E. coli* ATCC 25922	*P. aeruginosa* ATCC 27853	*C. albicans* ATCC 24433
$\mathbf{H_4L^1}$	6.0 ± 0	6.0 ± 0	6.0 ± 0	6.0 ± 0	6.0 ± 0
$\mathbf{H_3L^2}$	6.0 ± 0	6.0 ± 0	6.0 ± 0	6.0 ± 0	6.0 ± 0
1	6.0 ± 0	6.0 ± 0	6.0 ± 0	6.0 ± 0	6.0 ± 0
2	8.7 ± 0.2	6.5 ± 0.5	10.2 ± 0.2	11.0 ± 0.5	11.0 ± 1.0
3	6.0 ± 0	6.0 ± 0	6.0 ± 0	6.0 ± 0	6.0 ± 0
4	6.0 ± 0	6.0 ± 0	6.0 ± 0	6.0 ± 0	6.0 ± 0
5	6.0 ± 0	6.0 ± 0	6.0 ± 0	6.0 ± 0	6.0 ± 0
6	6.0 ± 0	6.0 ± 0	6.0 ± 0	6.0 ± 0	6.0 ± 0
7	10.5 ± 0.5	9.5 ± 0.5	11.0 ± 1.0	12.5 ± 0.5	15.5 ± 0.5
8	6.0 ± 0	6.0 ± 0	6.0 ± 0	6.0 ± 0	6.0 ± 0
9	6.0 ± 0	6.0 ± 0	6.0 ± 0	6.0 ± 0	6.0 ± 0

Table 4 MIC values of complexes 2 and 7 against a representative panel of reference strains. All the concentrations are expressed in μM

	S. aureus ATCC 29213		*E. faecalis* ATCC 29212		*E. coli* ATCC 25922		*P. aeruginosa* ATCC 27853		*C. albicans* ATCC 24433	
Compound	MIC	MBC	MIC	MBC	MIC	MBC	MIC	MBC	MIC	MBC
2	64–128	256	128	256	128	128	64	64	32	32
7	32	64	64	64	16	16	8	16	4	4

Conclusions

In the present work, for the new series of Co^{II}, $Co^{II,III}$, Cu^{II} and Ag^{I} complexes of AHBA and cocrystalline species with ethylenediamine and imidazole, we evaluated different biological properties such as anticancer and antimicrobial activity and DNA and BSA binding abilities. Among all the compounds screened, only the Ag^{I} complex (**7**) showed remarkable cytotoxic and antibacterial activity (higher of that of $AgNO_3$) while a lower activity was found for the cocrystalline (**2**), and no activity was revealed by the other tested derivatives. They are both different to all other proligands and metal complexes, in fact they seem to afford external electrostatic interactions with the DAPI–ct-DNA system without a displacement of the dye. Although the $Co^{II/III}$ complex **4** was able to bind strongly with DNA, it seems however to be not active towards the growth of tumor cells and bacteria.

Experimental

Materials and instrumentation

The ^1H and ^{13}C NMR spectra were recorded at room temperature on a Bruker Avance II + 300 (UltraShield™ Magnet) spectrometer operating at 300.130 and 75.468 MHz for proton and carbon-13, respectively. The chemical shifts are reported in ppm using tetramethylsilane as the internal reference. The infrared spectra (4000–400 cm^{-1}) were recorded on a BIO-RAD FTS 3000MX instrument in KBr pellets. Carbon, hydrogen, and nitrogen elemental analyses were carried out by the Microanalytical Service of the Instituto Superior Técnico. Electrospray mass spectra (ESI-MS) were run with an ion-trap instrument (Varian 500-MS LC Ion Trap Mass Spectrometer) equipped with an electrospray ion source. For electrospray ionization, the drying gas and flow rate were optimized according to the particular sample with 35 p.s.i. nebulizer pressure. Scanning was performed from *m*/*z* 100 to 1200 in methanol solution. The compounds were observed in the negative or positive mode (capillary voltage = 80–105 V).

Synthesis of H_3L^2

Diazotization. 2.55 g (20 mmol) of 4-chloroaniline was dissolved in 50 mL water, and 0.40 g (10 mmol) of NaOH was added. The solution was cooled in an ice bath to 273 K and 1.38 g (20 mmol) of $NaNO_2$ were added; 4.00 mL HCl were then added in 0.5 mL portions for 1 h. The temperature of the mixture should not exceed 278 K.

Azocoupling. NaOH (0.80 g, 20 mmol) was added to a mixture of 20 mmol (2.56 g) of barbituric acid with 50.00 mL of water. The solution was cooled in an ice bath, and a suspension of 4-chlorobenzenediazonium chloride (prepared according to the procedure described above) was added in two equal portions under vigorous stirring for 1 h. The formed precipitate of the H_3L^2 was filtered off, recrystallized from methanol and dried in air. The characterizations of the H_3L^2 was carried out by IR, ^1H and ^{13}C-NMR spectroscopies and are given below.

H_3L^2. Yield, 3.41 g, 64% (based on barbituric acid), yellow powder soluble in DMSO, methanol, acetone and acetonitrile. Anal. calcd for $C_{10}H_7ClN_4O_3$ (Mr = 266.64): C, 45.04; H, 2.65; N, 21.01; found: C, 44.87; H, 2.55; N, 20.83%. ESI-MS: *m*/*z*: 267.3 $[Mr + H]^+$. IR (KBr): 3260, 3085 and 2813 ν(NH), 1753 and 1653 ν(C=O), 1588 ν(C=O···H), 1513 ν(C=N) cm^{-1}. ^1H NMR (300.130 MHz) in DMSO-d_6, internal TMS, δ (ppm): 7.48–7.63 (4H, Ar-H), 11.31 (s, 1H, N–H), 11.52 (s, 1H, N–H), 14.03 (s, 1H, N–H). $^{13}C\{^1H\}$ NMR (75.468 MHz, DMSO-d_6). δ: 118.11 (Ar-Cl), 118.30 and 129.54 (4Ar-H), 129.70 (C=N), 140.46 (Ar-NHN=), 149.80 and 159.76 (C=O), 161.92 (C=O···H).

Synthesis of 2. A methanol solution (30 mL) of H_3L^2 (0.266 g, 1.0 mmol) was added at room temperature ethylenediamine (en) (0.06 mL, 1.0 mmol). The mixture was left for slow evaporation; the yellow-orange crystals of **2** suitable for X-rays started to form after *ca.* 1 d at room temperature; they were then filtered off and dried in air.

2: yield, 284 mg, 84% (based on H_3L^2). It is soluble in water, methanol, DMF, DMSO and only slightly in acetonitrile, acetone and chloroform. Anal. calcd for $C_{36}H_{49}Cl_3N_{18}O_{11}$ (Mr = 1016.25): C, 42.55; H, 4.86; N, 24.81; found: C, 42.27; H, 4.94; N, 24.88%. ESI-MS: *m*/*z*: 327.2 $[C_{12}H_{15}ClN_6O_3 + H]^+$. IR (KBr): 3446 and 3355 ν(OH), 3157 and 3062 ν(NH), 1693 and 1655 ν(C=O), 1579 ν(C=N) cm^{-1}. ^1H NMR (300.130 MHz) in DMSO-d_6, internal TMS, δ (ppm): 2.66 (4H, CH_2), 4.68 (6H, NH_3^+), 7.38–7.49 (4H, Ar-H). $^{13}C\{^1H\}$ NMR (75.468 MHz, DMSO-d_6). δ: 41.50 ($2CH_2$), 116.75 (Ar-Cl) and (Ar-NHN=), 120.13 (2Ar-H), 128.80 (2Ar-H), 129.10 (C=N), 149.06, 151.85 and 161.13 (C=O).

Synthesis of 7. 776 mg (1 mmol) of **1** were dissolved in water–acetone mixture (1 : 4, v/v), then 200 μL of HNO_3 (65% w/w) were added at room temperature. The addition of 338 mg (2 mmol) of $AgNO_3$ together with 10 mL of distilled water resulted in a clear solution. The resulting solution was allowed to stand in darkness room at room temperature and yellow crystals of **7** were obtained after 1 day.

7: yield, 236 mg, 54% (based on Ag). It is soluble in water, DMSO, methanol and DMF. Anal. calcd for $C_{10}H_9AgN_4O_7S$ (Mr = 437.13): C, 27.48; H, 2.08; N, 12.82%. Found: C, 27.51; H, 2.09;

N, 13.19%. IR (KBr): 3480 ν(OH), 3211 and 3067 ν(NH), 1736, 1689 and 1663 ν(C=O), 1579 ν(C=N) cm^{-1}. ESI-MS: m/z: 839.1 $[2Mr - 2H_2O + H]^+$. ^1H NMR (300.130 MHz) in DMSO-d_6, internal TMS, δ (ppm): 7.20–7.77 (4H, Ar-H), 11.21 (s, 1H, N–H), 11.33 (s, 1H, N–H), 14.78 (s, 1H, N–H). $^{13}C\{^1H\}$ NMR (75.468 MHz, DMSO-d_6). δ: 116.14, 118.16, 124.87 and 127.50 (Ar-H), 130.31 (Ar-NHN=), 135.96 (C=N), 138.16 (Ar-SO_3Ag), 150.00 and 160.22 (C=O), 160.62 (C=O···H).

Synthesis of 8. 776 mg (1 mmol) of **1** was dissolved in 30 mL methanol, then 200 μL of HNO_3 (65% w/w) and 136 mg (2 mmol) of imidazole (im) were added at room temperature. After *ca.* 1 d at room temperature, yellow crystals precipitated which were then filtered off and dried in air.

8: yield, 254 mg, 61% (based on im). It is soluble in water, methanol, DMF, DMSO and only slightly in acetonitrile, acetone and chloroform. Anal. calcd for $C_{13}H_{16}N_6O_8S$ (Mr = 416.37): C, 37.50; H, 3.87; N, 20.18%. Found: C, 37.26; H, 3.62; N, 20.20%. IR (KBr): 3446 ν(OH), 3202, 3063 and 2862 ν(NH), 1739, 1698 and 1675 ν(C=O), 1581 ν(C=N) cm^{-1}. ESI-MS: m/z: 312.1 $[H_3L^3 + H]^+$. ^1H NMR (300.130 MHz) in DMSO-d_6, internal TMS, δ (ppm): 7.19–7.77 (4H, Ar-H and 2H, *C*–H im), 9.08 (s, 1H, *C*–H im), 11.20 (s, 1H, N–H), 11.33 (s, 1H, N–H), 14.21 (s, 1H, N–H im), 14.79 (s, 1H, N–H). $^{13}C\{^1H\}$ NMR (75.468 MHz, DMSO-d_6). δ: 116.14, 118.16, 124.87 and 127.50 (Ar-H), 130.31 (Ar-NHN=), 135.96 (C=N), 138.16 (Ar-SO_3^-), 150.00 and 160.22 (C=O), 160.62 (C=O···H).

X-ray structure determinations

X-ray quality single crystals of the compounds were mounted in a nylon loop and measured at 150 K (**7** and **8**) or at room temperature (**2**). Intensity data were collected using a Bruker AXS-KAPPA APEX II diffractometer or a Bruker APEX-II PHOTON 100 diffractometer with graphite monochromated Mo-Kα (λ 0.71069) radiation. Data were collected using phi and omega scans of 0.5° per frame and a full sphere of data was obtained. Cell parameters were retrieved using Bruker SMART[41] software and refined using Bruker SAINT[49] on all the observed reflections. Absorption corrections were applied using SADABS.[49] Structures were solved by direct methods by using the SHELXS package[50] and refined with SHELXL-2014.[50] Calculations were performed using the WinGX System-Version 1.80.03.[51] The hydrogen atoms of water, hydrazine or ammonium groups were found in the difference Fourier map and the isotropic thermal parameters were set at 1.5 times the average thermal parameters of the belonging oxygen or nitrogen atoms, frequently with their distances restrained by using the DFIX and DANG commands. Coordinates of hydrogen atoms bonded to carbon atoms were included in the refinement using the riding-model approximation with the U_{iso}(H) defined as 1.2U_{eq} of the parent aromatic or methylene atoms. Least square refinements with anisotropic thermal motion parameters for all the non-hydrogen atoms and isotropic for the remaining atoms were employed. CCDC 1055318, 1055323 and 1055324 contain the supplementary crystallographic data for this paper.†

DNA interaction studies. A stock solution of calf thymus DNA (ct-DNA) (Sigma-Aldrich) was prepared by dissolving the solid material overnight in 10 mM phosphate buffer pH 7.2 containing 5 mM NaCl at 4 °C. The concentration of DNA was determined by UV absorbance at 260 nm as described.[52,53]

Electronic absorption titration. Calf thymus (ct) DNA binding experiments were performed in 10 mM and phosphate buffer pH 7.2 using DMSO solution of the complexes at room temperature. In UV-vis absorption titration phosphate buffer was used and the concentration of each complex was 13 μM while the ct-DNA concentration added was from 0 to 26 μM. The complex solution was titrated with the DNA, and changes on the intensity of the bands of the complex were monitored. The intrinsic binding constant (K_b) for the interaction of the complexes with ct-DNA was determined from a plot of [DNA]/($\varepsilon_a - \varepsilon_f$) *versus* [DNA] using absorption spectral titration data and the eqn (1):[54]

$$[DNA]/|\varepsilon_a - \varepsilon_f| = [DNA]/|\varepsilon_b - \varepsilon_f| + 1/K_b|\varepsilon_b - \varepsilon_f| \quad (1)$$

where [DNA] is the concentration of DNA, the apparent absorption coefficients ε_a, ε_f and ε_b correspond to A_{obsd}/[complex], the extinction coefficient for the free metal complex and the extinction coefficient for the metal complex in the fully bound form, respectively. The K_b value is given by the ratio of the slope to the intercept.

Fluorescence spectral study. The competitive binding experiment was carried out by maintaining the ethidium bromide (EB) (Sigma-Aldrich) and ct-DNA concentration at 5 μM and 50 μM, respectively, while increasing the concentration of different complexes (from a DMSO stock solution). Fluorescence quenching spectra were recorded using a Hitachi 4500 spectrofluorimeter with an excitation wavelength of 490 nm and 500–700 nm emission spectrum. The fluorescence spectra of a series of solutions with various concentrations of complex and a constant EB–ct-DNA complex were measured and the fluorescence value of decrease in emission spectra were corrected according to the relationship:

$$F_c = F_m \times e^{(A1+A2)/2} \quad (2)$$

where F_c and F_m are the corrected and measured fluorescence, respectively. $A1$ and $A2$ are the absorbance of tested compounds at the exciting and emission wavelengths. For fluorescence quenching experiments, the Stern–Volmer's equation was used (eqn (3)):

$$F_0/F_c = 1 + k_Q\tau_0[C] = 1 + K_{SV}[C] \quad (3)$$

where F_0 and F_c represent the fluorescence intensity in the absence and in the presence of drug. [C] is the concentration of complex and K_{SV} is the Stern–Volmer constant which is equal to $k_Q \times \tau_0$, where k_Q is the bimolecular quenching rate constant and τ_0 is the average fluorescence lifetime of the fluorophore in the absence of drug. All experiments involving ct-DNA were performed in buffer solution (10 mM phosphate buffer pH 7.2) at room temperature. The Stern–Volmer constant K_{SV} can be obtained by the eqn (4):[55]

$$I_0/I = 1 + K_{SV}[compound] \quad (4)$$

where I_0 and I are the emission intensities in the absence and presence of the compounds, respectively. K_{SV} depends on the ratio of the concentration of bound EB to the concentration of DNA and is called simply as the quenching constant.

The binding constant K_{app} was obtained by the eqn (5):

$$K_{EB}[EB] = K_{app}[compound] \quad (5)$$

in which the compound concentration is the value at a 50% reduction of the fluorescence intensity of EB and $K_{EB} = 1.0 \times 10^7$ M^{-1} ([EB] = 5.0 μM).[56]

Minor groove displacement assay. A well-known minor groove binder, 4′,6-diamidino-2-phenylindole (DAPI), was used to perform the minor groove displacement assays as reported earlier. In a typical experiment, the changes in the emission spectra of DAPI complex with the DNA in 10 mM phosphate buffer pH 7.2, were monitored upon addition of increasing concentrations of compounds at room temperature. Fluorescence quenching data were evaluated after excitation of DAPI–ct-DNA complex at 338 nm and recording the spectra from 400–600 nm. Values of K_{SV} constants were evaluated using eqn (3) after that all quenching fluorescence values obtained were corrected according to the relationship (2). In the presence of enhancement of fluorescence the values of K_{SV} was evaluate as previously described.[57,58]

BSA binding studies. The protein-binding study was performed by tryptophan fluorescence quenching experiments using bovine serum albumin (BSA). Bovine serum albumin (Sigma-Aldrich) stock solutions were prepared in 20 mM potassium phosphate buffer pH 7.4. Fluorescence measurements were carried out with a Hitachi 4500 spectrofluorometer by keeping the concentration of BSA constant (15×10^{-6} M) while varying the complex concentration (from 0 to 40×10^{-6} M), at room temperature. Fluorescence intensities were recorded after each successive addition of complex solution and equilibration (*ca.* 5 min). Fluorescence spectra were recorded from 300 to 450 nm at an excitation wavelength of 285 nm. The value of Stern–Volmer constants and association binding constant of the different metal complexes to HSA were evaluated following the eqn (3) and fluorescent values were corrected by eqn (2).

Antiproliferative activity. A375 (human malignant melanoma cell line) and MDA-MB 231 cells (human breast adenocarcinoma cell line) were cultured in Dulbecco's Modified Eagle's Medium (DMEM) with 2 mM L-glutamine, 100 IU mL^{-1} penicillin, 100 μg mL^{-1} streptomycin, and supplemented with 10% heat-inactivated foetal bovine serum (HI-FBS). HCT116 cells (human colon carcinoma cell line) were cultured in RPMI1640 medium with 2 mM L-glutamine, 100 IU mL^{-1} penicillin, 100 μg mL^{-1} streptomycin, and supplemented with 10% HI-FBS. Cells were cultured in a humidified atmosphere at 37 °C in the presence of 5% CO_2. The MTT assay was used as a relative measure of cell viability. Cell-viability assays were carried out as described. Briefly, cells were seeded at the density of 2×10^4 cells per mL. After 24 h, samples were exposed to different concentrations of compounds **1–9** (0.39–100 μM). Cells were incubated for 72 h in a humidified atmosphere of 5% CO_2 at 37 °C. At the end of incubation, the cytotoxic activity was evaluated by the MTT assay.[32b] Experiments were conducted in triplicate. Cytotoxicity is expressed as the concentration of compound inhibiting cell growth by 50% (IC_{50}). The IC_{50} values were determined with GraphPad Prism 4 computer program (GraphPad Software, S. Diego, CA, USA). Analysis of variance was performed in InStat, GraphPad software, San Diego CA, USA. Unpaired t test was used for these analyses, and $p < 0.001$ was considered to be statistically significant.

Antimicrobial activity. The antimicrobial activity of ligands, cocrystals and complexes was determined by both disc diffusion and by microdilution methods following the general guidelines of the Clinical Laboratory Standard Institute (CLSI).[59] Microorganisms included in this study were: *Staphylococcus aureus* ATCC 29213, *Escherichia coli* ATCC 25922, *Pseudomonas aeruginosa* ATCC 27853, *Enterococcus faecalis* ATCC 29212, *Candida albicans* ATCC 24433. Bacterial strains were cultured overnight at 37 °C on blood agar plates and *C. albicans* was grown in RPMI1640. For the disk diffusion method a suspension of 10^8 cells per mL prepared in saline (10^6 per mL for *C. albicans*) was spread on the solid media plates (MHA for bacteria and MH supplemented with 2% glucose and 0.5 mg mL^{-1} of methylene blue for *Candida*) using a sterile cotton swab. Sterile filter paper discs (6 mm in diameter) were placed on the surface of inoculated plates and spotted with 10 μL of each compound (20 mM in DMSO). The plates were incubated for 24 h at 35 ± 2 °C (48 h in the case of *Candida*). The known antimicrobials ciprofloxacin (5 μg per disc) and nystatin (100 U per disc) (CLSI) were used as positive control against bacteria and fungus, respectively. Activity was determined by measuring the diameter of the growth inhibition zone (inhibition zone diameter, IZD) visible around the paper disc (expressed in mm) using a caliper. Reported IZDs are inclusive of the paper disc diameter (6 mm). Therefore, a 6 mm IZD means no activity. No zone of inhibition was observed using DMSO alone. Each test was repeated three times. For the microdilution method two-fold serial dilutions of each compound were prepared in 96-well plates, starting from 256 μM in Cation Adjusted Mueller Hinton Broth or RPMI 1640 medium, depending on the microorganism tested. An equal volume of bacterial (10^6 cfu mL^{-1}) or fungal (10^3 cfu mL^{-1}) inoculum was added to each well of the microtiter plate containing 0.1 mL of the serially diluted test molecule. Incubation followed for 18–24 h at 35 °C (24–48 h in the case of *C. albicans*) in a normal atmosphere. The Minimum Inhibitory Concentrations (MICs) were defined as the lowest concentration of the compound able to inhibit the growth of the microorganisms. All tests were done in triplicate. Minimum Bactericidal Concentration (MBC) was subsequently determined as recommended by the CLSI guidelines.

Acknowledgements

This work has been partially supported by the Foundation for Science and Technology (FCT), Portugal (UID/QUI/00100/2013 project). M. F. C. G. S. and A. J. L. P. acknowledge the Russian Science Foundation for support in the structural analysis and

help in organizing the International Laboratory (grant 14-43-00017). The authors acknowledge the Portuguese NMR Network (IST-UTL Centre) for access to the NMR facility, and the IST Node of the Portuguese Network of mass-spectrometry (Dr Conceição Oliveira) for the ESI-MS measurements. The authors also acknowledge the financial support by the University of Camerino (Fondo di Ateneo per la Ricerca 2011–2012) and Nuova Simonelli Company.

References

1 C. J. Suckling, in *Trends in Medicinal Chemistry*, ed. H. van der Goot, G. Domany, L. Pallos and H. Timmerman, Elsevier, Amsterdam, 1989, p. 805.
2 E. Maquoi, N. E. Sounni, L. Devy, F. Olivier, F. Frankenne, H.-W. Krell, F. Grams, J.-M. Foidart and A. Noel, *Clin. Cancer Res.*, 2004, **10**, 4038–4047.
3 H.-J. Breyholz, S. Wagner, A. Faust, B. Riemann, C. Hoeltke, S. Hermann, O. Schober, M. Schafersa and K. Kopka, *ChemMedChem*, 2010, **5**, 777–789.
4 P. Bartsch, D. Cataldo, R. Endele, B. Evrard, J.-M. Foidart, H.-W. Krell and G. Zimmermann, Int. Appl. No. PCT EP, 003348, 2005.
5 F. Grams, H. Brandstetter, S. D'Alo, D. Geppert, H.-W. Krell, H. Leinert, V. Livi, E. Menta, A. Oliva and G. Zimmermann, *Biol. Chem.*, 2001, **382**, 1277–1285.
6 K. T. Mahmudov, M. N. Kopylovich, A. M. Maharramov, M. M. Kurbanova, A. V. Gurbanov and A. J. L. Pombeiro, *Coord. Chem. Rev.*, 2014, **265**, 1–37.
7 K. T. Mahmudov, M. N. Kopylovich and A. J. L. Pombeiro, *Coord. Chem. Rev.*, 2013, **257**, 1244–1281.
8 K. T. Mahmudov, M. F. C. Guedes da Silva, M. Glucini, M. Renzi, K. C. P. Gabriel, M. N. Kopylovich, M. Sutradhar, F. Marchetti, C. Pettinari, S. Zamponi and A. J. L. Pombeiro, *Inorg. Chem. Commun.*, 2012, **22**, 187–189.
9 C. Saravanan, S. Easwaramoorthi and L. Wang, *Dalton Trans.*, 2014, **43**, 5151–5157.
10 M. Klikar, F. Bureš, O. Pytela, T. Mikysek, Z. Padělková, A. Barsella, K. Dorkenoo and S. Achelle, *New J. Chem.*, 2013, **37**, 4230–4240.
11 M. Szostak, B. Sautier and D. J. Procter, *Chem. Commun.*, 2014, **50**, 2518–2521.
12 H. D. Williams, N. L. Trevaskis, S. A. Charman, R. M. Shanker, W. N. Charman, C. W. Pouton and C. J. H. Porte, *Pharmacol. Rev.*, 2013, **65**, 315–499.
13 C. A. Lipinski, *Curr. Drug Discovery Technol.*, 2001, **4**, 17–19.
14 C. A. Lipinski, *Am. Pharm. Rev.*, 2002, **5**, 82–85.
15 E. M. Merisko-Liversidge and G. G. Liversidge, *Toxicol. Pathol.*, 2008, **36**, 43–48.
16 L. S. Reddy, N. J. Babu and A. Nangia, *Chem. Commun.*, 2006, 1369–1371.
17 R. V. Prasad, M. G. Rakesh, R. M. Jyotsna, S. T. Mangesh, P. S. Anita and P. K. Mayur, *Int. J. Pharm., Chem. Biol. Sci.*, 2012, **1**, 725–736.
18 J. Palmucci, K. T. Mahmudov, M. F. C. Guedes da Silva, L. M. D. R. S. Martins, F. Marchetti, C. Pettinari and A. J. L. Pombeiro, *RCS Adv.*, 2015, **5**, 84142–84152.
19 A. M. Maharramov, R. A. Aliyeva, I. A. Aliyev, F. G. Pashaev, A. G. Gasanov, S. I. Azimova, R. K. Askerov, A. V. Kurbanov and K. T. Mahmudov, *Dyes Pigm.*, 2010, **85**, 1–6.
20 K. T. Mahmudov, A. M. Maharramov, R. A. Aliyeva, I. A. Aliyev, R. K. Askerov, R. Batmaz, M. N. Kopylovich and A. J. L. Pombeiro, *J. Photochem. Photobiol., A*, 2011, **219**, 159–165.
21 S. R. Gadjieva, T. M. Mursalov, K. T. Mahmudov and F. M. Chyragov, *Russ. J. Coord. Chem.*, 2006, **32**, 304–308.
22 K. T. Mahmudov, R. A. Aliyeva, S. R. Gadjieva and F. M. Chyragov, *J. Anal. Chem.*, 2008, **63**, 435–438.
23 A. W. Addison, T. N. Rao, J. Reedijk, J. van Rijn and G. C. Verschoor, *J. Chem. Soc., Dalton Trans.*, 1984, 1349–1356.
24 Y. Gülseven, E. Taşal, İ. Sıdır, T. Güngör, H. Berber and C. Öğretir, *Int. J. Hydrogen Energy*, 2009, **34**, 5255–5259.
25 A. Airinei, E. Rusu and D. Dorohoi, *Spectrosc. Lett.*, 2001, **34**, 65–74.
26 İ. Sıdır, E. Taşal, Y. Gülseven, T. Güngör, H. Berber and C. Öğretir, *Int. J. Hydrogen Energy*, 2009, **34**, 5267–5273.
27 R. S. Kumar, K. Sasikala and S. Arunachalam, *J. Inorg. Biochem.*, 2008, **102**, 234–241.
28 Z.-C. Liu, B.-D. Wang, B. Li, Q. Wang, Z.-Y. Yang, T.-R. Li and Y. Li, *Eur. J. Med. Chem.*, 2010, **45**, 5353–5361.
29 K. Akdi, R. A. Vilaplana, S. Kamah and F. González-Vílchez, *J. Inorg. Biochem.*, 2005, **99**, 1360–1368.
30 Q. Li, P. Yang, H. Wang and M. Guo, *J. Inorg. Biochem.*, 1996, **64**, 181–195.
31 S. Shi, J. Liu, J. Li, K.-C. Zheng, X.-M. Huang, C.-P. Tan, L.-M. Chen and L.-N. Ji, *J. Inorg. Biochem.*, 2006, **100**, 385–395.
32 (*a*) S. Tabassum, M. Afzal and F. Arjmand, *J. Photochem. Photobiol., B*, 2012, **115**, 63–72; (*b*) S. Tabassum, M. Zaki, M. Afzal and F. Arjmand, *Eur. J. Med. Chem.*, 2014, **74**, 509–523.
33 F. J. Meyer-Almes and D. Porschke, *Biochemistry*, 1993, **32**, 4246–4253.
34 J. B. LePecq and C. Paoletti, *J. Mol. Biol.*, 1967, **27**, 87–106.
35 R. F. Pasternack, M. Cacca, B. Keogh, T. A. Stephenson, A. P. Williams and F. J. Gibbs, *J. Am. Chem. Soc.*, 1991, **113**, 6835–6840.
36 E. N. Zaitsev and S. C. Kowalczykowski, *Nucleic Acids Res.*, 1998, **26**, 650–654.
37 P. Smoleński, C. Pettinari, F. Marchetti, M. F. C. Guedes da Silva, G. Lupidi, G. V. Badillo Pazmay, D. Petrelli, L. A. Vitali and A. J. L. Pombeiro, *Inorg. Chem.*, 2015, **54**, 434–440.
38 A. Pabbathi and A. Samanta, *J. Phys. Chem. B*, 2015, **119**, 11099–11105.
39 M. Shamsi, S. Yadav and F. Arjmand, *J. Photochem. Photobiol., B*, 2014, **136**, 1–11.
40 J. Lu, A. J. Stewart, P. J. Sadler, T. J. Pinheiro and C. A. Blindauer, *Biochem. Soc. Trans.*, 2008, **36**, 1317–1321.
41 A. M. Merlot, D. S. Kalinowski and D. R. Richardson, *Front. Physiol.*, 2014, **12**, 1–7, ID 299.
42 O. K. Abou-Zied and O. I. K. Al-Shihi, *J. Am. Chem. Soc.*, 2008, **130**, 10793–10801.

43 D. Senthil Raja, N. S. P. Bhuvanesh and K. Natarajan, *Inorg. Chem.*, 2011, **50**, 12852–12866.
44 M. Tan, W. Liang, X. Luo and Y. Y. Gu, *J. Chem.*, 2013, 1–6, ID 308054.
45 J. Jayabharathi, K. Jayamoorthy, V. Thanikachalam and R. Sathishkumar, *Spectrochim. Acta, Part A*, 2013, **108**, 146–150.
46 (*a*) X. Zhang, L. Li, Z. Xu, Z. Liang, J. Su, J. Huang and B. Li, *PLoS One*, 2013, **8**, e59106; (*b*) H. Cao, D. Wu, H. Wang and M. Xu, *Spectrochim. Acta, Part A*, 2009, **73**, 972–975.
47 I. Timtcheva, V. Maximova, T. Deligeorgiev, N. Gadjev, K. H. Drexhage and I. Petkova, *J. Photochem. Photobiol., B*, 2000, **58**, 130–135.
48 W. R. Ware, *J. Phys. Chem.*, 1962, **66**, 455–458.
49 Bruker, *APEX2 & SAINT*, AXS Inc., Madison, WI, 2004.
50 G. M. Sheldrick, *Acta Crystallogr., Sect. A: Found. Crystallogr.*, 2008, **64**, 112–122.
51 L. J. Farrugia, *J. Appl. Crystallogr.*, 1999, **32**, 837–838.
52 S. Tabassum, S. Amir, F. Arjmand, C. Pettinari, F. Marchetti, N. Masciocchi, G. Lupidi and R. Pettinari, *Eur. J. Med. Chem.*, 2013, **60**, 216–232.
53 A. Wolfe, G. H. Shimer and T. Meehan, *Biochemistry*, 1987, **26**, 6392–6396.
54 A. M. Pyle, J. P. Rehmann, R. Meshoyrer, C. V. Kumar, N. J. Turro and J. K. Barton, *J. Am. Chem. Soc.*, 1989, **111**, 3051–3058.
55 O. Stern and M. Volmer, *Z. Med. Phys.*, 1919, **20**, 183–188.
56 M. Lee, A. L. Rhodes, M. D. Wyatt, S. Forrow and J. A. Hartley, *Biochemistry*, 1993, **32**, 4237–4245.
57 N. Shahabadi, M. Maghsudi, M. Mahdavi and M. Pourfoulad, *DNA Cell Biol.*, 2012, **31**, 122–127.
58 L. Quassinti, F. Maggi, L. Barboni, M. Ricciutelli, M. Cortese, F. Papa, C. Garulli, C. Kalogris, S. Vittori and M. Bramucci, *Fitoterapia*, 2014, **97**, 133–141.
59 CLSI, *Performance standards for antimicrobial susceptibility testing, 19th informational supplement M100-S19*, Clinical and Laboratory Standards Institute, Wayne, PA, 2009, p. 20.